NASA/TM–2002–211750

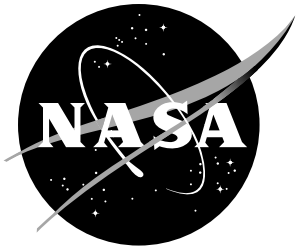

Elliptic Relaxation of a Tensor Representation for the Redistribution Terms in a Reynolds Stress Turbulence Model

J. R. Carlson and T. B. Gatski
Langley Research Center, Hampton, Virginia

July 2002

The NASA STI Program Office ... in Profile

Since its founding, NASA has been dedicated to the advancement of aeronautics and space science. The NASA Scientific and Technical Information (STI) Program Office plays a key part in helping NASA maintain this important role.

The NASA STI Program Office is operated by Langley Research Center, the lead center for NASA's scientific and technical information. The NASA STI Program Office provides access to the NASA STI Database, the largest collection of aeronautical and space science STI in the world. The Program Office is also NASA's institutional mechanism for disseminating the results of its research and development activities. These results are published by NASA in the NASA STI Report Series, which includes the following report types:

- TECHNICAL PUBLICATION. Reports of completed research or a major significant phase of research that present the results of NASA programs and include extensive data or theoretical analysis. Includes compilations of significant scientific and technical data and information deemed to be of continuing reference value. NASA counterpart and peer-reviewed formal professional papers, but having less stringent limitations on manuscript length and extent of graphic presentations.

- TECHNICAL MEMORANDUM. Scientific and technical findings that are preliminary or of specialized interest, e.g., quick release reports, working papers, and bibliographies that contain minimal annotation. Does not contain extensive analysis.

- CONTRACTOR REPORT. Scientific and technical findings by NASA-sponsored contractors and grantees.

- CONFERENCE PUBLICATION. Collected papers from scientific and technical conferences, symposia, seminars, or other meetings sponsored or co-sponsored by NASA.

- SPECIAL PUBLICATION. Scientific, technical, or historical information from NASA programs, projects, and missions, often concerned with subjects having substantial public interest.

- TECHNICAL TRANSLATION. English-language translations of foreign scientific and technical material pertinent to NASA's mission.

Specialized services that complement the STI Program Office's diverse offerings include creating custom thesauri, building customized databases, organizing and publishing research results...even providing videos.

For more information about the NASA STI Program Office, see the following:

- Access the NASA STI Program Home Page at ***http://www.sti.nasa.gov***

- E-mail your question via the Internet to help@sti.nasa.gov

- Fax your question to the NASA STI Help Desk at (301) 621–0134

- Phone the NASA STI Help Desk at (301) 621–0390

- Write to:
  NASA STI Help Desk
  NASA Center for AeroSpace Information
  7121 Standard Drive
  Hanover, MD 21076–1320

NASA/TM–2002–211750

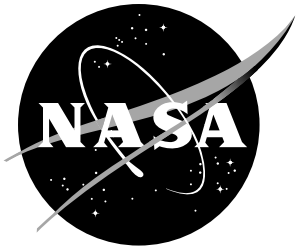

Elliptic Relaxation of a Tensor Representation for the Redistribution Terms in a Reynolds Stress Turbulence Model

J. R. Carlson and T. B. Gatski
Langley Research Center, Hampton, Virginia

National Aeronautics and
Space Administration

Langley Research Center
Hampton, Virginia 23681–2199

July 2002

Available from:

NASA Center for AeroSpace Information (CASI)
7121 Standard Drive
Hanover, MD 21076–1320
(301) 621–0390

National Technical Information Service (NTIS)
5285 Port Royal Road
Springfield, VA 22161–2171
(703) 605–6000

Elliptic Relaxation of a Tensor Representation for the Redistribution Terms in a Reynolds Stress Turbulence Model

J.R.CARLSON AND *T.B.GATSKI*
Computational Modeling & Simulation Branch
NASA Langley Research Center, Hampton, VA 23681, USA

Abstract

A formulation to include the effects of wall proximity in a second-moment closure model that utilizes a tensor representation for the redistribution terms in the Reynolds stress equations is presented. The wall-proximity effects are modeled through an elliptic relaxation process of the tensor expansion coefficients that properly accounts for both correlation length and time scales as the wall is approached. Direct numerical simulation data and Reynolds stress solutions using a full differential approach are compared to the tensor representation approach for the case of fully developed channel flow.

1. INTRODUCTION

The theoretical development of higher order closure models, such as Reynolds stress models, have primarily been formulated based on high Reynolds number assumptions. The influence of solid boundaries on these closure models has usually been accounted for through either a wall function approach or a modification to the high Reynolds number form of the pressure-related correlations and tensor dissipation rate and predicated on the near-wall asymptotic behavior of the various velocity second moments (So et al. 1991, Hanjalić 1994).

A broader based attempt to account for the proximity of a solid boundary is the elliptic relaxation approach introduced over a decade ago (Durbin 1991) and further developed for second-moment closures (Durbin 1993a, Wizman et al. 1996; Manceau and Hanjalić 2000, Manceau, Carlson and Gatski 2001). In its two-equation form the $v^2 - f$ model has been applied to a variety of flows (e.g., Durbin 1993b, 1995; Pettersson Reif et al. 1999). The new approach outlined here introduces a tensor representation for the combined effects of a near-wall velocity-pressure gradient correlation and anisotropic dissipation rate that asymptotes to a high Reynolds number form away from solid boundaries through an elliptic equation for the polynomial expansion coefficients. The development of a generalized methodology for determining the polynomial expansion coefficients of representations for the turbulent stress anisotropies by (Gatski and Jongen 2000) is extended to an elliptic relaxation procedure for these expansion coefficients.

Although the material presented here introduces tensor representations and a tensor projection methodology into the elliptic relaxation formulation, this work can also be viewed as an intermediate step between a fully explicit elliptic relaxation algebraic Reynolds stress formulation and the full differential elliptic relaxation Reynolds stress formulation.

The predictive capabilities of the new model are assessed through comparisons with direct numerical simulation channel flow data (Moser et al. 1999). These comparisons include both mean and turbulent flow quantities.

2. Theoretical Background and Development

In this section, a mathematical framework is developed for the Reynolds stress transport equations and the corresponding elliptic relaxation equation when a tensor representation of the redistribution terms is used in the formulation. The methodology introduces a set of elliptic relaxation equations for the polynomial expansion coefficients of the chosen representation. The $\boldsymbol{\tau} - \mathbf{f}$ model uses the redistributive terms in the elliptic equations, while the $\boldsymbol{\tau} - \beta_n$ model uses the expansion coefficients in the elliptic equations. Both models use the Reynolds stress transport equations.

2.1 Transport Equations

The transport of the Reynolds stresses τ_{ij} $(= -\overline{u_i u_j})$ is governed by the equation

$$\frac{D\tau_{ij}}{Dt} = -\tau_{ik}\frac{\partial U_j}{\partial x_k} - \tau_{jk}\frac{\partial U_i}{\partial x_k} + \phi_{ij} - \varepsilon_{ij} + \mathcal{D}^T_{ij} + \mathcal{D}^\nu_{ij}, \tag{1}$$

where U_i is the mean velocity, ϕ_{ij} is the pressure redistribution term, ε_{ij} is the tensor dissipation rate, and $\mathcal{D}^T_{ij}$ and $\mathcal{D}^\nu_{ij}$ are the turbulent transport and viscous diffusion, respectively. In the development outlined here, it is best to have ϕ_{ij} given by

$$\phi_{ij} = -\overline{u_i\frac{\partial p}{\partial x_j}} - \overline{u_j\frac{\partial p}{\partial x_i}} + \frac{2}{3}\frac{\partial\,\overline{pu}_k}{\partial x_k}\delta_{ij}, \tag{2}$$

so that the trace of the pressure redistribution term is zero. In the application of the elliptic relaxation method, it is also necessary to account for the effect of the dissipation rate anisotropy as the wall is approached. This accounting for the dissipation rate anisotropy is accomplished (e.g., Manceau 2000) by a relaxation of the dissipation rate anisotropy to its wall value, which is assumed to be equal to the Reynolds stress anisotropy. This assumption allows the Reynolds stress transport equation in (1) to be written as

$$\frac{D\tau_{ij}}{Dt} = -\tau_{ik}\frac{\partial \overline{U}_j}{\partial x_k} - \tau_{jk}\frac{\partial \overline{U}_i}{\partial x_k} + \varepsilon K f_{ij} - \frac{\tau_{ij}}{K}\varepsilon + \mathcal{D}^T_{ij} + \mathcal{D}^\nu_{ij}, \tag{3}$$

where

$$\varepsilon K f_{ij} = \phi_{ij} - 2\varepsilon\left(d_{ij} - b_{ij}\right), \tag{4}$$

with the Reynolds stress anisotropy b_{ij} and dissipation rate anisotropy d_{ij} defined as

$$b_{ij} = \frac{\tau_{ij}}{2K} - \frac{\delta_{ij}}{3}, \qquad d_{ij} = \frac{\varepsilon_{ij}}{2\varepsilon} - \frac{\delta_{ij}}{3}. \tag{5}$$

The original scaling of the relaxation function f_{ij} was solely through the turbulent kinetic energy K; however, Manceau, Carlson and Gatski (2001) have recently shown

that an added dissipation rate factor, ε, to the scaling $(\varepsilon K f_{ij})$ eliminates an unwanted amplification effect inherent in the original scaling.

Equation (3) is closed when the model for the turbulent transport $\mathcal{D}_{ij}^T$ is used. In previous elliptic relaxation studies that used the Reynolds stress transport equations, the viscous diffusion and turbulent transport terms were modeled as

$$\mathcal{D}_{ij}^{\nu} = \nu\nabla^2\tau_{ij}, \quad \mathcal{D}_{ij}^T \equiv -\frac{\partial}{\partial x_k}\left(\overline{u_i u_j u_k} + \frac{2}{3}\overline{p u_k}\right) = \frac{\partial}{\partial x_l}\left(C_\mu \frac{\tau_{lk}}{\sigma_K}\tau_c \frac{\partial \tau_{ij}}{\partial x_k}\right), \tag{6}$$

with $\sigma_K = 1.0$ and $C_\mu = 0.15$. The composite time scale

$$\tau_c = \max\left[\tau, C_{\tau_K}\left(\frac{\nu}{\varepsilon}\right)^{1/2}\right], \qquad \tau = \frac{K}{\varepsilon}, \tag{7}$$

where $C_{\tau_K} = 6$ determines the switch to the Kolmogorov time scale $(\nu/\varepsilon)^{1/2}$ so that the turbulent time scale will not vanish as the solid boundary is approached. Away from the boundary, the composite time scale asymptotes to the inertial scale K/ε.

In the two-dimensional flow considered here, solutions were obtained for the τ_{11} and τ_{22} normal Reynolds stresses and the τ_{12} shear stress. A transport equation for the turbulent kinetic energy was obtained from one-half the trace of Eq. (3) and was solved for in lieu of the third normal stress τ_{33},

$$\frac{DK}{Dt} = \mathcal{P} - \varepsilon + \frac{\partial}{\partial x_l}\left(C_\mu \frac{\tau_{lk}}{\sigma_K}\tau_c \frac{\partial K}{\partial x_k}\right) + \nu\nabla^2 K, \tag{8}$$

where $\mathcal{P} = \tau_{ik}\partial U_i/\partial x_k$. The modeled transport equation for the turbulent dissipation rate ε needed for closure is given by

$$\frac{D\varepsilon}{Dt} = \frac{1}{\tau_c}\left(C_{\varepsilon 1}^{*}\mathcal{P} - C_{\varepsilon 2}\varepsilon\right) + \frac{\partial}{\partial x_l}\left(C_\mu \frac{\tau_{lk}}{\sigma_\varepsilon}\tau_c \frac{\partial \varepsilon}{\partial x_k}\right) + \nu\nabla^2\varepsilon \tag{9}$$

where $\sigma_\varepsilon = 1.3$, $C_{\varepsilon 1} = 1.44$, $C_{\varepsilon 2} = 1.83$, with

$$C_{\varepsilon 1}^{*} = C_{\varepsilon 1}\left(1 + a_1\frac{\mathcal{P}}{\varepsilon}\right), \quad a_1 = 0.09. \tag{10}$$

Note that this form of the dissipation rate equation (Durbin 1991) has introduced the composite time scale into both the production and destruction of dissipation terms.

2.2 Elliptic Relaxation Methodology: $\boldsymbol{\tau - \mathrm{f}}$ Model

The rescaled elliptic relaxation equation is driven by the high Reynolds number form of the pressure-strain rate correlation $\mathbf{\Pi}$ and a contribution from the Reynolds stress anisotropy $2\varepsilon_c b_{ij}$ (away from the wall the dissipation rate is assumed to be isotropic $d_{ij} = 0$). This combination results in an elliptic relaxation equation for f_{ij} given by (cf. Manceau and Hanjalić 2000)

$$\left(1 - L^2\nabla^2\right) f_{ij} = \frac{1}{\varepsilon K}\left(\Pi_{ij}^h + 2\varepsilon_c b_{ij}\right) \equiv f_{ij}^h \tag{11}$$

where

$$\varepsilon_c = \frac{K}{\tau_c}, \tag{12}$$

and the relaxation scales are defined as

$$L = C_L \max\left[\frac{K^{3/2}}{\varepsilon}, C_{L_K}\left(\frac{\nu}{\varepsilon}\right)^{1/4}\right], \tag{13}$$

with $C_L = 0.16$ and $C_{L_K} = 80$. Previous implementations of the elliptic relaxation procedure (Manceau and Hanjalić 2000) using the Speziale, Sarkar and Gatski (SSG) pressure strain rate model (Speziale et al. 1991) used the full nonlinear form. The linear form of the SSG model implemented here is given by

$$\begin{aligned}\Pi_{ij}^h = &-\left(C_1^0\varepsilon_c + C_1^1\mathcal{P}\right)b_{ij} + KC_2S_{ij} + KC_3\left(b_{ik}S_{kj} + S_{ik}b_{kj} - \frac{2}{3}b_{nm}S_{nm}\delta_{ij}\right)\\ &-KC_4\left(b_{ik}W_{kj} - W_{ik}b_{kj}\right)\end{aligned} \tag{14}$$

with $C_1^0 = 1.8$, $C_1^1 = 3.4$, $C_2 = 0.37$, $C_3 = 1.25$, and $C_4 = 0.4$. Note that since the linear form of the pressure-strain rate model is used here, the value for C_L differs from that used previously ($C_L = 0.2$, see Manceau and Hanjalić 2000) for the form of the elliptic relaxation equation given in (11).

Boundary conditions are needed for the f_{ij} and are determined, in the vicinity of the wall, by the balance of the redistributive term by the viscous diffusion of the Reynolds stresses resulting in Table 1. Only the 22- and 12-components of $\mathbf{f}$ have determinate solutions to the near-wall balance of the stress transport equations. For the remaining components $f_{11} = f_{33} = -f_{22}/2$ are used as boundary conditions to ensure that f_{ij} is traceless (Manceau, Carlson and Gatski 2001). Symmetry conditions were applied at the centerline.

In the current work, one of the goals is to develop a methodology for incorporating a tensor representation for the relaxed redistribution function f_{ij}. Once developed and validated this same procedure can be used in conjunction with tensor representations for the Reynolds stress anisotropies as well. Such a combination would then yield an elliptic relaxation explicit algebraic stress model. The details of the representation for the Reynolds stress anisotropy will not be addressed in the current work, but deserves further work. As will be discussed in Sec. 2.3, such a representation would be consistent with a linear pressure-strain rate model.

2.3 Representations and Elliptic Relaxation: $\boldsymbol{\tau} - \beta_n$ Model

Although the elliptic relaxation formulation has already been applied within a full differential Reynolds stress model, a question arises about what role tensor representations can play within the framework of the elliptic relaxation procedure.

Table 1. Boundary Conditions for the f_{ij} Tensor

Component	Wall	Centerline
f_{11}	$-\frac{1}{2}f_{22,w}$	Symmetry
f_{22}	$\frac{-20\nu^2\tau_{22}\Big\vert_1}{\varepsilon_w^2 y_1^4}$	Symmetry
f_{33}	$-\frac{1}{2}f_{22,w}$	Symmetry
f_{12}	$\frac{-20\nu^2\tau_{12}\Big\vert_1}{\varepsilon_w^2 y_1^4}$	0

The differential elliptic relaxation equation for f_{ij} can be obtained from the integral expression (e.g. Manceau and Hanjalić, 2000)

$$f_{ij}(\mathbf{x}) = \frac{1}{\varepsilon(\mathbf{x})K(\mathbf{x})}\left\{\phi_{ij}(\mathbf{x}) - 2\varepsilon(\mathbf{x})\left[d_{ij}(\mathbf{x}) - b_{ij}(\mathbf{x})\right]\right\} = \int_\Omega d^3\mathbf{x}'\left[\frac{F_{ij}(\mathbf{x},\mathbf{x}')}{\varepsilon(\mathbf{x})K(\mathbf{x})}\right] G_\Omega(\mathbf{x},\mathbf{x}'), \tag{15}$$

where

$$\begin{aligned} F_{ij}(\mathbf{x},\mathbf{x}') = & \underbrace{-u_i(\mathbf{x})\nabla^2\frac{\partial p}{\partial x_j}(\mathbf{x}') - u_j(\mathbf{x})\nabla^2\frac{\partial p}{\partial x_i}(\mathbf{x}') + \frac{2}{3}\delta_{ij}u_k(\mathbf{x})\nabla^2\frac{\partial p}{\partial x_k}(\mathbf{x}')}_{\text{velocity}-\text{pressure gradient correlation}} \\ & + \frac{1}{2}\Bigg\{ \underbrace{2\nu\left(\frac{\partial u_i}{\partial x_l}(\mathbf{x})\nabla^2\frac{\partial u_j}{\partial x_l}(\mathbf{x}') + \frac{\partial u_j}{\partial x_l}(\mathbf{x})\nabla^2\frac{\partial u_i}{\partial x_l}(\mathbf{x}')\right)}_{\text{tensor dissipation rate}} \\ & - \frac{\varepsilon(\mathbf{x})}{K(\mathbf{x})}\underbrace{\left[u_i(\mathbf{x})\nabla^2 u_j(\mathbf{x}') + u_j(\mathbf{x})\nabla^2 u_i(\mathbf{x}')\right]}_{\text{Reynolds stress tensor}}\Bigg\} \end{aligned} \tag{16}$$

and $G_\Omega(\mathbf{x},\mathbf{x}')$ is approximated by the free-space Greens function $G_\Omega(\mathbf{x},\mathbf{x}') = (4\pi r)^{-1}$ with $r = \|\mathbf{x}' - \mathbf{x}\|$. The δ_{ij} contributions to both the dissipation rate and Reynolds stress anisotropies cancel so that the only remaining contributions are the tensor dissipation rate and Reynolds stress tensor. The tensor function f_{ij} and $\mathcal{F}_{ij}$ can be represented by polynomial expansions of basis tensors just as the associated Reynolds stress anisotropy tensor b_{ij} has been. For such a basis given by $T_{ij}^{(m)}(\mathbf{x})$ $(m = 1,\ldots,\mathrm{N})$, the following representations are assumed:

$$f_{ij}(\mathbf{x}) = \sum_{l=1}^{\mathrm{N}} \beta_l(\mathbf{x}) T_{ij}^{(l)}(\mathbf{x}) \tag{17}$$

$$F^*_{ij}(\mathbf{x},\mathbf{x}') \;=\; \frac{F_{ij}(\mathbf{x},\mathbf{x}')}{\varepsilon(\mathbf{x})K(\mathbf{x})} = \sum_{n=1}^{\mathrm{N}} \gamma_n(\mathbf{x},\mathbf{x}')T^{(n)}_{ij}(\mathbf{x}). \tag{18}$$

A tensor scalar product (denoted by [:]) between each basis tensor $T^{(m)}_{ij}(\mathbf{x})$ and the representations given in Eqs. (17) and (18) can be formed, and this leads (using matrix notation for convenience) to

$$\begin{aligned}\sum_{l=1}^{\mathrm{N}} \beta_l(\mathbf{x}) \left[\mathbf{T}^{(l)}(\mathbf{x}){:}\mathbf{T}^{(m)}(\mathbf{x})\right] &= \int_\Omega d^3\mathbf{x}' \left[\mathbf{F}^*(\mathbf{x},\mathbf{x}'){:}\mathbf{T}^{(m)}(\mathbf{x})\right] G_\Omega(\mathbf{x},\mathbf{x}') \\ &= \sum_{n=1}^{\mathrm{N}} \int_\Omega d^3\mathbf{x}'\gamma_n(\mathbf{x},\mathbf{x}') \left[\mathbf{T}^{(n)}(\mathbf{x}){:}\mathbf{T}^{(m)}(\mathbf{x})\right] G_\Omega(\mathbf{x},\mathbf{x}') \end{aligned} \tag{19}$$

Since the functional dependency of the indicated scalar product depends solely on $\mathbf{x}$, Eq. (19) can be rewritten as

$$\beta_n(\mathbf{x}) = \int_\Omega d^3\mathbf{x}'\gamma_n(\mathbf{x},\mathbf{x}')G_\Omega(\mathbf{x},\mathbf{x}'). \tag{20}$$

The modeling of the scalar function $\gamma_n(\mathbf{x},\mathbf{x}')$ follows that established previously for the elliptic relaxation approach, that is

$$\gamma_n(\mathbf{x},\mathbf{x}') = \gamma_n(\mathbf{x}',\mathbf{x}') \exp\left(-\frac{r}{L_n}\right). \tag{21}$$

where, in general, the γ_n coefficients can have an associated length scale uniquely defined by the form given in Eq. (13).

With this model, Eq. (20) can be rewritten as

$$\beta_n(\mathbf{x}) = \int_\Omega d^3\mathbf{x}'\gamma_n(\mathbf{x}',\mathbf{x}')\frac{\exp\left(-r/L_n\right)}{4\pi r}. \tag{22}$$

This equation leads directly to the differential counterpart

$$\left(1 - L_n^2\nabla^2\right)\beta_n(\mathbf{x}) = -L_n^2\gamma_n(\mathbf{x},\mathbf{x}) = \beta^h_n(\mathbf{x}), \tag{23}$$

where $\beta^h_n(\mathbf{x})$ are the expansion coefficients from the tensor representation of a quasi-homogeneous form of $\mathbf{f}$. Since the dissipation rate is assumed to be isotropic, $\mathbf{f}$ is composed of the quasi-homogeneous form of the pressure-strain rate correlation and a contribution due to the Reynolds stress anisotropy. The resultant expression for $\beta^h_n(\mathbf{x})$ is given by

$$\begin{aligned}\sum_{n=1}^{\mathrm{N}} \beta^h_n(\mathbf{x}) \left[\mathbf{T}^{(n)}(\mathbf{x}){:}\mathbf{T}^{(m)}(\mathbf{x})\right] &= \frac{1}{\varepsilon(\mathbf{x})K(\mathbf{x})} \left[\left(\mathbf{\Pi}^h(\mathbf{x}) + 2\varepsilon_c\mathbf{b}(\mathbf{x})\right){:}\mathbf{T}^{(m)}(\mathbf{x})\right] \\ &= \frac{\left[\mathbf{\Pi}^h_c(\mathbf{x}){:}\mathbf{T}^{(m)}(\mathbf{x})\right]}{\varepsilon(\mathbf{x})K(\mathbf{x})}, \qquad m = 1,\ldots\mathrm{N}, \end{aligned} \tag{24}$$

where the quasi-homogeneous form of the pressure-strain rate model $\mathbf{\Pi}_c^h$ is given by

$$\mathbf{\Pi}_c^h = -\varepsilon_c \left(C_1^0 - 2 + C_1^1 \frac{\mathcal{P}}{\varepsilon} \right) \mathbf{b} + KC_2 \mathbf{S} + KC_3 \left(\mathbf{bS} + \mathbf{Sb} - \frac{2}{3}[\mathbf{b}{:}\mathbf{S}]\mathbf{I} \right) - KC_4 \left(\mathbf{bW} - \mathbf{Wb} \right). \quad (25)$$

Note that a comparison of Eqs. (14) and (25) shows that the return-to-isotropy term proportional to $\mathbf{b}$ has been modified. The factor ε_c now influences the entire term and the contribution from the Reynolds stress anisotropy $2\varepsilon_c\mathbf{b}$ to the relaxation function $\mathbf{f}$ is now included in this (slow) term contribution to $\mathbf{\Pi}_c^h$.

One of the improvements in the current elliptic relaxation formulation is that the scaled relaxation function $\mathbf{f}$ defined in Eq. (4) is $\mathcal{O}(1)$ in the log-layer region. This scaling negates the adverse influence of the elliptic operator in the log-layer that occurred in the original (Durbin 1993a) formulation. In order to retain this benign effect in the tensor representation formulation used here, it is necessary to ensure that the expansion coefficients β_n also have this neutral effect.

Previous representations for the Reynolds stress anisotropy tensor have used basis tensors of the form $\mathbf{S}$, $\mathbf{SW} - \mathbf{WS}$, and $\mathbf{S}^2 - [\mathbf{S}{:}\mathbf{S}]\mathbf{I}/3$. In the log-layer, where the velocity gradient has a y^{-1} behavior, this choice of basis tensors would require that the corresponding expansion coefficients β_1, β_2, and β_3 have a y, y^2, and y^2 behavior, respectively, in that region to ensure that $\mathbf{f}$ behaves as $\mathcal{O}(1)$. Unfortunately, given that behavior of the β_n, the amplification effect would now effect the β_n and the sought-after $\mathcal{O}(1)$ behavior for the $\mathbf{f}$ is lost. For the fully developed channel flows of interest, this problem can be easily circumvented by using a normalized basis set of the form

$$\mathbf{T}^{(1)} = \mathbf{S}^*, \quad \mathbf{T}^{(2)} = \mathbf{S}^*\mathbf{W}^* - \mathbf{W}^*\mathbf{S}^*, \quad \mathbf{T}^{(3)} = \mathbf{S}^{*2} - \frac{\mathbf{I}}{3}, \quad (26)$$

where $\mathbf{S}^* = \mathbf{S}/\{\mathbf{S}^2\}^{1/2}$ and $\mathbf{W}^* = \mathbf{W}/\{\mathbf{S}^2\}^{1/2}$. This normalization now makes the behavior of both the expansion coefficients and basis tensors $\mathcal{O}(1)$ in the log-layer, which then precludes any adverse effect of the elliptic operator in the relaxation equation (23).

Boundary conditions for the β_n expansion coefficients are required. Consistent with the boundary conditions for the tensor function f_{ij}, the corresponding β_n boundary conditions are listed in Table 2 as functions of τ_{ij} (see Appendix A for details).

The equivalence of the elliptic relaxation of the expansion coefficients β_n given by Eq. (23) with the elliptic relaxation of the function f_{ij} given by Eq. (11) can be readily shown with the current normalized basis. The solution to Eq. (24) is easily obtained as

$$\begin{aligned} \left(\beta_1^h,\ \beta_2^h,\ \beta_3^h\right) &= \frac{1}{\varepsilon K} \left([\mathbf{\Pi}_c^h{:}\mathbf{T}^{(1)}],\ [\mathbf{\Pi}_c^h{:}\mathbf{T}^{(2)}],\ [\mathbf{\Pi}_c^h{:}\mathbf{T}^{(2)}] \right) \\ &= \frac{1}{\varepsilon K} \left(\sqrt{2}\Pi_{c12}^h,\ \frac{1}{2}(\Pi_{c22}^h - \Pi_{c11}^h),\ 3(\Pi_{c11}^h + \Pi_{c22}^h) \right). \end{aligned} \quad (27)$$

Table 2. Boundary Conditions for β_n

β_n	Wall	Centerline
β_1	$\dfrac{-20\sqrt{2}\nu^2\ \tau_{12}\big\vert_{(1)}}{\varepsilon_w^2 y_{(1)}^4}$	$\dfrac{[\mathbf{\Pi}_c{:}\mathbf{T}^{(1)}]^h}{\varepsilon K}$
β_2	$\dfrac{-15\nu^2\ \tau_{22}\big\vert_{(1)}}{\varepsilon_w^2 y_{(1)}^4}$	$\dfrac{[\mathbf{\Pi}_c{:}\mathbf{T}^{(2)}]^h}{\varepsilon K}$
β_3	$\dfrac{-30\nu^2\ \tau_{22}\big\vert_{(1)}}{\varepsilon_w^2 y_{(1)}^4}$	$\dfrac{[\mathbf{\Pi}_c{:}\mathbf{T}^{(3)}]^h}{\varepsilon K}$

If the tensor representation Eq. (17) is applied to f_{ij}^h, then the β_n solution from Eq. (27) would yield for the components of f_{ij}^h

$$\left(f_{12}^h,\ f_{11}^h,\ f_{22}^h,\ f_{33}^h\right) = \left(\frac{\beta_1^h}{\sqrt{2}},\ -\beta_2^h + \frac{\beta_3^h}{6},\ \beta_2^h + \frac{\beta_3^h}{6},\ -\frac{\beta_3^h}{3}\right)$$

$$= \frac{1}{\varepsilon K}\left(\Pi_{c12}^h,\ \Pi_{c11}^h,\ \Pi_{c22}^h,\ \Pi_{c33}^h\right). \tag{28}$$

A comparison of the right-hand side of Eq. (28) with the right-hand side of Eq. (11) shows that the two are equivalent. (The reader should recall from the discussion following the definition of $\mathbf{\Pi}_c^h$ in Eq. (25) that the form of the slow term was slightly modified from the definition given in Eq. (14). With this change taken into account, the exact equivalence Eqs. (11) and (28) holds.)

3. Results and Discussion

All flow calculations were carried out on fully developed turbulent channel flows. The equations that were solved were scaled in wall units with friction Reynolds number Re_τ based on channel half-height and friction velocity at the wall. A one-dimensional finite-difference algorithm described in Appendix B was used for all computations.

As shown in Sec. 2.3, the representation methodology that has been developed yields an elliptic relaxation formulation equivalent to the elliptic relaxation of the tensor function f_{ij}. While such tensor projection methods have been used in conjunction with nonlinear algebraic equations, the application here also validates its use with differential operators.

Figures 1 – 3 show the predictive accuracy and equivalence of both the $\tau_{ij} - f_{ij}$ and $\tau_{ij} - \beta_n$ approaches. The flow field is the fully developed channel flow at $Re_\tau = 590$ (Moser et al. 1999). The figures include both a linear and log scale in the wall normal direction. As can be seen from Fig. 1 for the mean velocity, both the distribution across the channel and the near-wall asymptotic behavior agree with

the direct numerical simulation (DNS) data. Excellent agreement with the DNS data

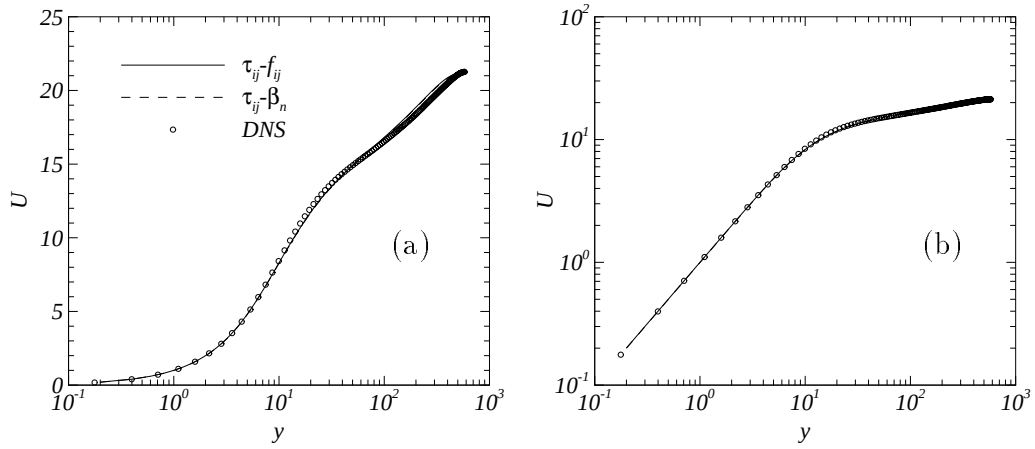

Figure 1. Mean velocity distribution across channel at $Re_\tau = 590$: (a) log-linear scale; (b) log-log scale.

across the channel is also shown for the shear stress profile (Fig. 2); however, the asymptotic approach to the wall is greater than the theoretical estimate of $\mathcal{O}(y^3)$. The discrepancy becomes apparent for values of $y < 1$. This result is in contrast to the predictions for the turbulent kinetic energy shown in Fig. 3. In this case

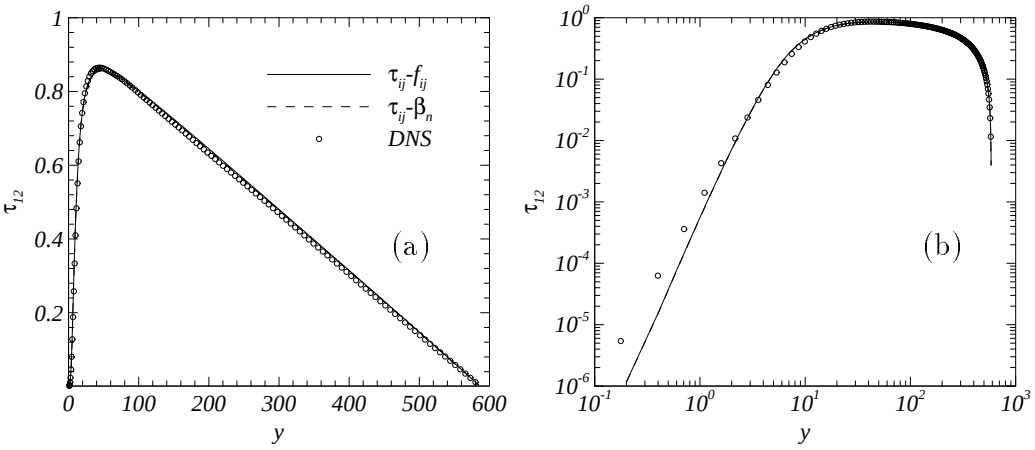

Figure 2. Turbulent shear stress distribution across channel at $Re_\tau = 590$: (a) linear scale; (b) log-log scale.

the near-wall asymptotic behavior is consistent with the DNS results but the overall values are slightly lower across the channel than the DNS data. Overall, the predictive results for the mean velocity, Reynolds shear stress and turbulent kinetic energy are quite exceptional and show that the method can be calibrated to provide excellent predictions of this flow field. In actuality, since the models are formally equivalent, no changes are required in any of the calibration constants.

Since a full differential Reynolds stress model is used for the turbulent velocity field, it is possible as well as insightful to further examine the component stress predictions. Figures 4 and 5 show the τ_{11} and τ_{22} component stresses. Since the

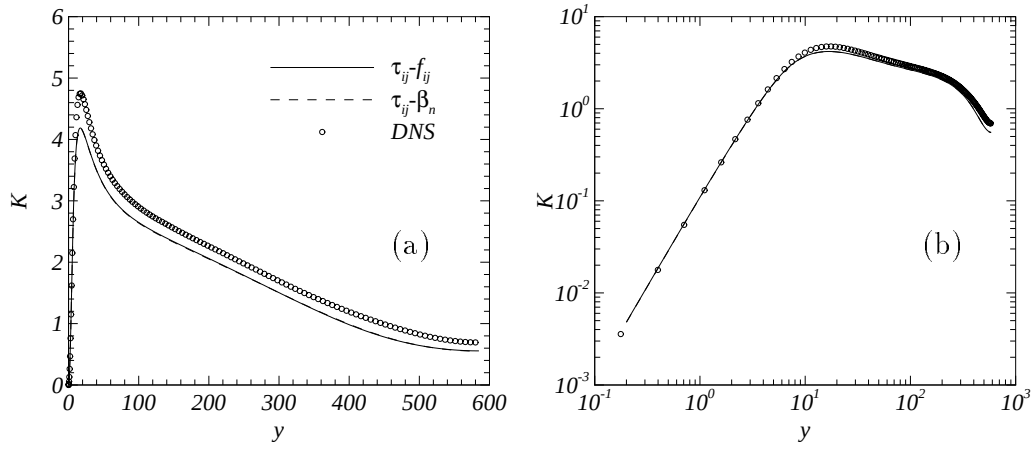

Figure 3. Turbulent kinetic energy distribution across channel at $Re_\tau = 590$: (a) linear scale; (b) log-log scale.

near-wall asymptotic behavior $\mathcal{O}(y^2)$ is dominated by the τ_{11} (and τ_{33}) components, it is not surprising to see from Fig. 4b that the near-wall asymptotics closely match the DNS results. The $\mathcal{O}(y^4)$ behavior that characterizes the DNS results for the τ_{22} component (see Fig. 5b) are very closely replicated by the predictions. Fig. 4a shows that across the channel predicted results were lower than the DNS results for the τ_{11} component. For the τ_{22} component, however, the predicted peak value was higher than the DNS results, but the predicted values were lower over the remainder of the channel, as seen in Fig. 5a.

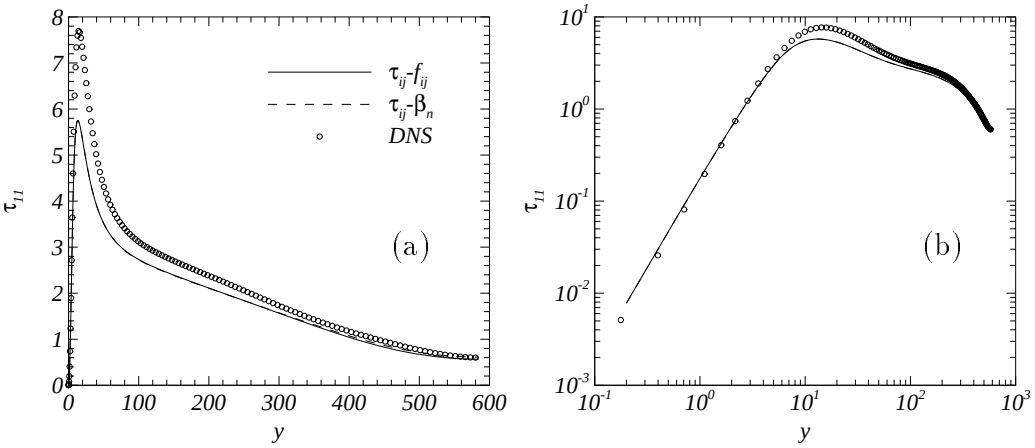

Figure 4. Reynolds normal stress component τ_{11} distribution across channel at $Re_\tau = 590$: (a) linear scale; (b) log-log scale.

An interesting assessment of how well the elliptic relaxation formulation models the redistribution terms across the channel can be obtained from Eq. (4). The quantity $\varepsilon K f_{ij}$ obtained from the explicit representation given in Eq. (18) and the elliptically relaxed β_n from Eq. (23) are plotted in Fig. 6 along with the quantity $\phi_{ij} - 2\varepsilon(d_{ij} - b_{ij})$ obtained from the DNS data. As Fig. 6a shows, the $\varepsilon K f_{12}$ component produces the corresponding DNS results very well in the near-wall region and in the

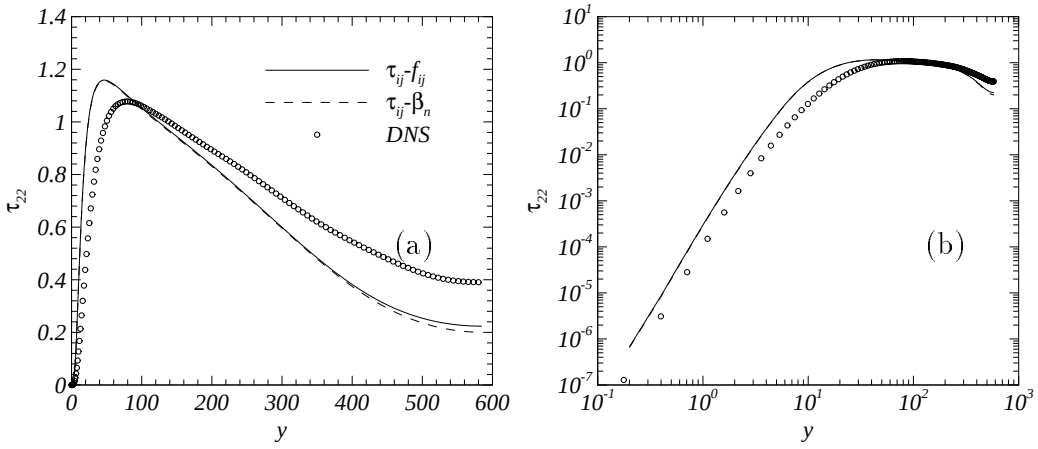

Figure 5. Reynolds normal stress component τ_{22} distribution across channel at Re_τ = 590: (a) linear scale; (b) log-log scale.

outer layer region toward the centerline. Between these two regions, the peak value of the computations greatly exceeds that of the DNS. The normal $\varepsilon K f_{11}$ and $\varepsilon K f_{22}$ components show an even poorer prediction of the DNS results. In these cases, only the outer layer region is correctly predicted; whereas, over the rest of the channel the qualitative and quantitative predictions are generally poor. While the results of this *a priori* validation of the elliptically relaxed function $\varepsilon K f_{ij}$ are disappointing, it is clear that the actual predictions of the fully modeled set of equations are generally very good. Thus other modeled terms in the formulation are able to account for any discrepancies in the prediction of the redistribution term.

As Fig. 6 shows, all components of the elliptically relaxed redistribution term correctly reproduce the DNS data in the outer layer of the channel flow but differ extensively from the DNS data when reproducing the inner layer. Since the elliptic operator term $(-L^2\nabla^2)$ is responsible for the deviation of the β_n from their quasi-homogeneous β_n^h forms, it is worthwhile to quantify the size of the region across the channel that is affected by this term. Figure 7 shows the distribution of $-L^2\nabla^2\beta_n$ across the channel for the three expansion coefficients $(n = 1, 2, 3)$ at three different values of Re_τ. In the inner layer, the wall unit scaling basically collapses the results for all values of Re_τ, with the exception of the β_1 component where the results in the near-wall region show some dependence on Re_τ; this sensitivity to Re_τ is not found in the other components as Figs. 7b and 7c show. The effect of the elliptic operator falls to zero at y (wall unit) values around 10^2. The overshoot in the outer layer shown in all the figures is attributed to the asymptotic behavior of the energy dissipation rate ε in this region. Both $\nabla^2\beta_n$ and ε decrease (L increases); however, the dissipation rate ε decreases faster (L increases faster) than the corresponding decrease in $\nabla^2\beta_n$. The variation with Re_τ in this region is not surprising since the wall unit scaling is not the proper scaling for this region.

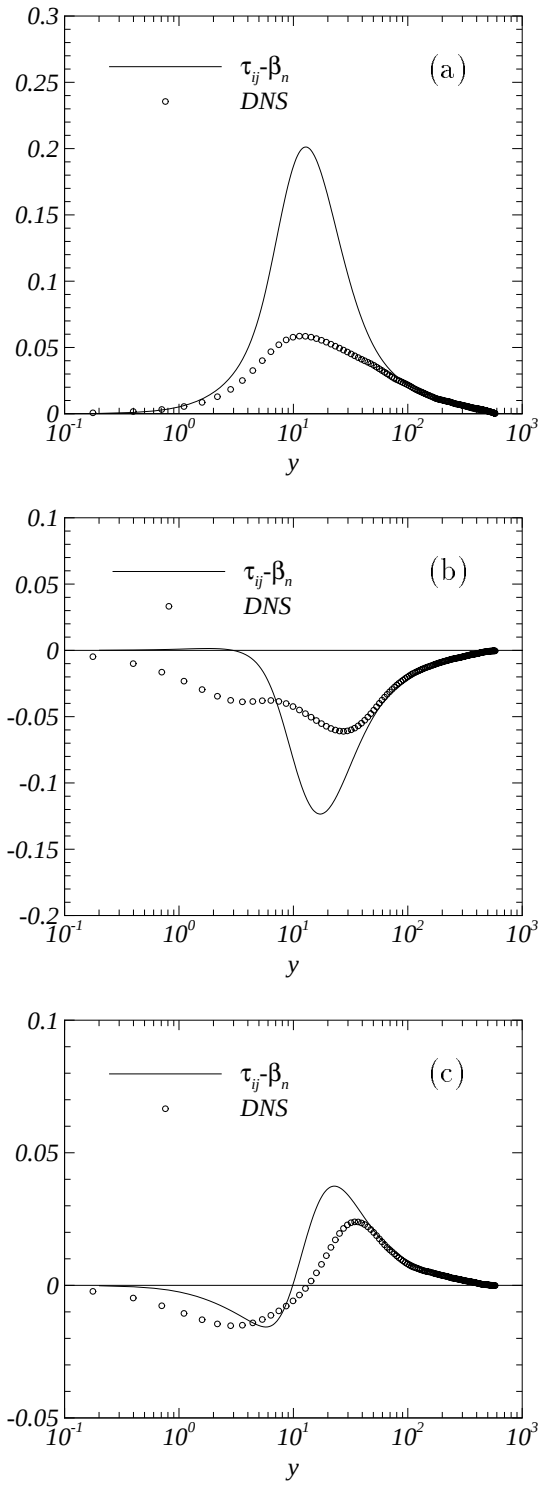

Figure 6. Comparison of predicted redistribution term components with DNS data at $Re_\tau = 590$: (a) 12-component, (b) 11-component, (c) 22-component. For all components $\tau_{ij} - \beta_n$ results are $\varepsilon K f_{ij}$, and DNS results are $\phi_{ij} - 2\varepsilon(d_{ij} - b_{ij})$.

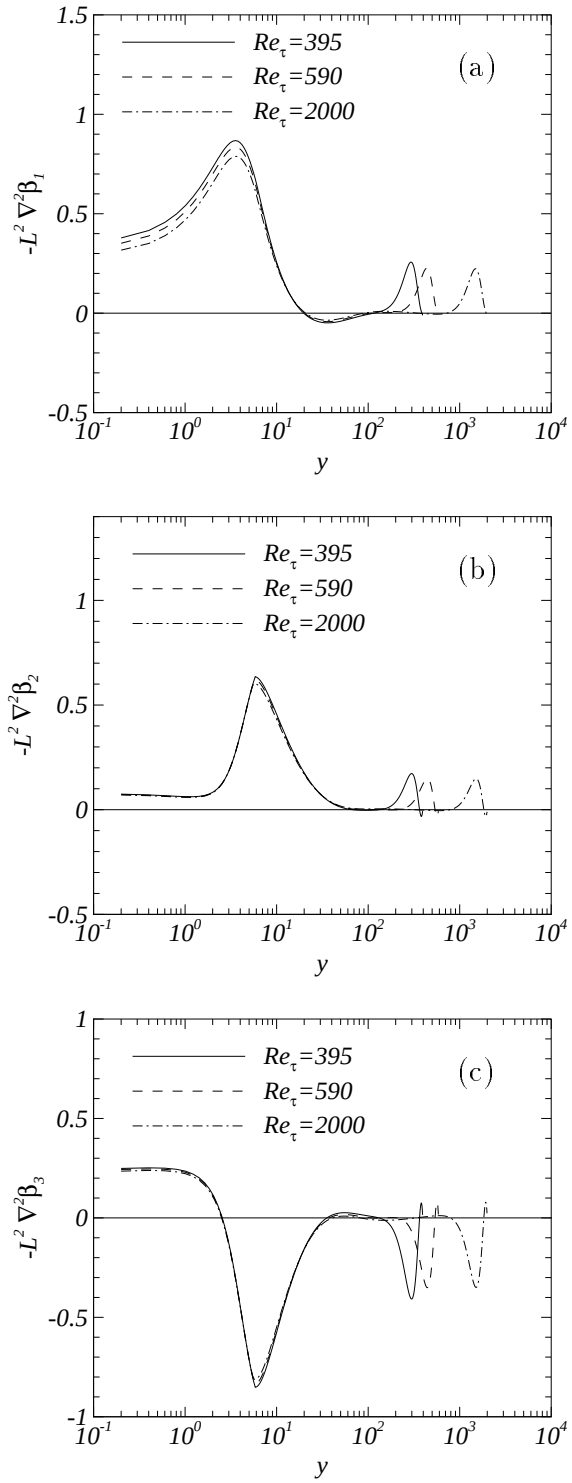

Figure 7. Effect of elliptic operator across channel at different Re_τ: (a) β_1-coefficient, (b) β_2-coefficient, (c) β_3-coefficient.

4. Summary

A methodology has been developed that introduces a polynomial representation for the tensor redistribution function f_{ij}. An elliptic relaxation equation, analogous to the f_{ij} relaxation equation is formulated for the polynomial expansion coefficients β_n. The new prediction method is demonstrated on a fully developed channel flow problem and gives similar results to the previous elliptic relaxation method for f_{ij}. A formal equivalence is established between the elliptic relaxation of the tensor function f_{ij} and its tensor representation. Although the predictions of the mean velocity and turbulent stresses are generally accurate over the channel, an *a priori* assessment shows that the current formulation does not model the redistribution well. Such results are enlightening but are not uncommon; the results reflect the fact that in modeled closure schemes, a combination of modeled terms combine to yield predictions of quantities such as the mean velocity and Reynolds stresses.

While the theoretical approach developed here does not result in a reduction in computational cost, it does introduce a new methodology that is requisite for developing elliptic relaxation explicit algebraic stress models. The next step in the development of such models will be to introduce representations for the Reynolds stress anisotropies and analyze the effects of modeling the turbulent transport and viscous diffusion terms consistent with the approximations made in the formulation of algebraic stress models.

Acknowledgment

The authors are indebted to Dr. Remi Manceau for several useful discussions during the course of this work.

Appendix A β_n Boundary Conditions

The expressions for the β_n boundary conditions are derived from the basis tensors $T_{ij}^{(n)}$ used in the representation of f_{ij}

$$f_{ij} = \sum_{n=1}^{3} \beta_n \hat{T}_{ij}^{(n)} \rightarrow \begin{cases} f_{11} = \beta_2 T_{11}^{(2)} + \beta_3 T_{11}^{(3)} \\ f_{22} = \beta_2 T_{22}^{(2)} + \beta_3 T_{22}^{(3)} \\ f_{33} = \beta_3 T_{33}^{(3)} \\ f_{12} = \beta_1 T_{12}^{(1)} \end{cases} \tag{A1}$$

Table 1 gives the corresponding boundary conditions for these f_{ij} components. The boundary condition for β_1 is directly proportional to the f_{12} boundary condition and is given by

$$\beta_{1,w} = \frac{f_{12,w}}{T_{12}^{(1)}} = \sqrt{2} f_{12,w} = \frac{-20\sqrt{2}\nu^2 \tau_{12}}{\varepsilon_w^2 y_{(1)}^4} \tag{A2}$$

The coefficient β_3 appears in all three expansions of the diagonal terms of f_{ij}. If f_{ij} is traceless, a unique expression for β_3 at the wall will be obtained. From the representation for f_{33}, $\beta_{3,w}$ can be immediately written as

$$\beta_{3,w} = \frac{f_{33,w}}{T_{33,w}^{(3)}} = -3 f_{33,w} = \frac{-30\nu^2 \tau_{22}}{\varepsilon_w^2 y_{(1)}^4} \tag{A3}$$

The representations for f_{11} and f_{22} can be used to obtain an equivalent expressions for the β_3 boundary condition

$$\beta_{3,w} = \frac{f_{22,w} T_{11,w}^{(2)} - f_{11,w} T_{22,w}^{(2)}}{T_{22,w}^{(3)} T_{11,w}^{(2)} - T_{11,w}^{(3)} T_{22,w}^{(2)}} = -\frac{(f_{22,w} + f_{11,w})}{T_{33,w}^{(3)}} = -3 f_{33,w} \tag{A4}$$

With $\beta_{3,w}$ known, the representation for either f_{11} or f_{22} can be used to obtain $\beta_{2,w}$. From the f_{22} representation, the wall boundary condition on β_2 is given by

$$\begin{aligned} \beta_{2,w} &= \frac{\left(f_{22,w} - T_{22,w}^{(3)} \beta_{3,w}\right)}{T_{22,w}^{(2)}} \\ &= \frac{\left(f_{22,w} + 3 f_{33,w} T_{22,w}^{(3)}\right)}{\hat{T}_{22,w}^{(2)}} = f_{22,w} + \frac{f_{33,w}}{2} = \frac{-15\nu^2 \tau_{22}}{\varepsilon_w^2 y_{(1)}^4} \end{aligned} \tag{A5}$$

Appendix B Numerical Solution Methodology

A one-dimensional finite-difference code was used for all computations. All equations were normalized by the bulk viscosity and friction velocity (i.e., wall units). The differencing template was node-centered with clustering close to the wall using an exponential stretching function. In terms of the scaling used for the channel flow calculations, the 500 node grid had the first point at a height of 0.1 wall units. The channel Reynolds number Re_τ determined the channel grid height. The K and ε equations were implicitly coupled as were the $\tau_{ij} - f_{ij}$ equations, and for the second model, the $\tau_{ij} - \beta_n$ equations. The variables U, K, ε and τ_{ij} were solved in a time-dependent mode, while the f_{ij} or β_l equations were not (*i.e.*, $\Delta t = 0.$) All variables were updated at each time step.

In this appendix, the terms with the superscript $(n+1)$ denote variables that were implicitly solved for and the terms with the superscript (n) were variables used explicitly at each iteration. The Reynolds stress equations coupled implicitly with either the f_{ij} or β_n equations were solved first, with the momentum, turbulent kinetic energy and dissipation rate equations solved second. An updated τ_{12} was used in the momentum equation, but the eddy viscosity in the turbulent transport terms of all the equations was not updated until after the completion of each time step. Typically solutions were re-started from previous turbulent flow calculations.

The symbol y_1 denotes the height of the first node from the wall and ε_w denotes the boundary condition value for ε. The discretized form of the governing equations are as follows. For the $\boldsymbol{\tau} - \mathbf{f}$ model;

$$\tau_{ij}^{(n+1)} = \tau_{ij}^{(n)} + \Delta t \Bigg[P_{ij}^{(n)} + \varepsilon^{(n)} K^{(n)} f_{ij}^{(n+1)} - \frac{\tau_{ij}^{(n+1)}}{K^{(n)}} \varepsilon^{(n)} + \frac{d}{dy}\left(\left(1 + \frac{\nu_t^{(n)}}{\sigma_K} \right) \frac{d}{dy} \tau_{ij}^{(n+1)} \right) \Bigg] \tag{B1}$$

$$f_{ij}^{(n+1)} - L^{(n)^2} \frac{d^2}{dy^2} f_{ij}^{(n+1)} = \frac{1}{\varepsilon^{(n)} K^{(n)}} \left(\Pi_{ij}^h + 2\varepsilon_c b_{ij} \right)^{(n)}. \tag{B2}$$

The boundary conditions were implicitly written for the f_{ij} as

$$f_{22}^{(n+1)}\Big|_w = -20 \frac{\tau_{22}^{(n+1)}\big|_{y_1}}{\varepsilon_w^{(n)^2} y_1^4} \tag{B3}$$

$$f_{11}^{(n+1)}\Big|_w = 10 \frac{\tau_{22}^{(n+1)}\big|_{y_1}}{\varepsilon_w^{(n)^2} y_1^4} \tag{B4}$$

$$f_{12}^{(n+1)}\Big|_w = -20 \frac{\tau_{12}^{(n+1)}\big|_{y_1}}{\varepsilon_w^{(n)^2} y_1^4}. \tag{B5}$$

For the $\boldsymbol{\tau} - \beta_l$ model;

$$\tau_{ij}^{(n+1)} = \tau_{ij}^{(n)} + \Delta t \Bigg[P_{ij}^{(n)} + \varepsilon^{(n)} K^{(n)} \left(\sum_{l=1}^{N} \beta_l^{(n+1)} \hat{T}_{ij}^{(l)} \right) - \frac{\tau_{ij}^{(n+1)}}{K^{(n)}} \varepsilon^{(n)} + \frac{d}{dy} \left(\left(1 + \frac{\nu_t^{(n)}}{\sigma_K} \right) \frac{d}{dy} \tau_{ij}^{(n+1)} \right) \Bigg] \tag{B6}$$

$$\beta_l^{(n+1)} - L^{(n)^2} \frac{d^2}{dy^2} \beta_l^{(n+1)} = \frac{1}{\varepsilon^{(n)} K^{(n)}} \left(\frac{\left[\mathbf{\Pi}_c^h : \mathbf{T}^{(m)} \right]}{\left[\mathbf{T}^{(l)} : \mathbf{T}^{(m)} \right]} \right)^{(n)} . \tag{B7}$$

Similarly, the boundary conditions were implicitly written for the β_l as

$$\beta_1^{(n+1)} \Big|_w = -20\sqrt{2} \frac{\tau_{12}^{(n+1)} \big|_{y_1}}{\varepsilon_w^{(n)^2} y_1^4} \tag{B8}$$

$$\beta_2^{(n+1)} \Big|_w = -15 \frac{\tau_{22}^{(n+1)} \big|_{y_1}}{\varepsilon_w^{(n)^2} y_1^4} \tag{B9}$$

$$\beta_3^{(n+1)} \Big|_w = -30 \frac{\tau_{22}^{(n+1)} \big|_{y_1}}{\varepsilon_w^{(n)^2} y_1^4} . \tag{B10}$$

For U, K and ε;

$$U^{(n+1)} = U^{(n)} + \Delta t \left[-\frac{dp}{dx} + \frac{d}{dy} U^{(n+1)} + \frac{d}{dy} \tau_{12}^{(n+1/2)} \right], \quad -\frac{dp}{dx} = \frac{1}{Re_\tau} \tag{B11}$$

$$K^{(n+1)} = K^{(n)} + \Delta t \left[\mathcal{P}^{(n)} - \varepsilon^{(n+1)} + \frac{d}{dy} \left(\left(1 + \frac{\nu_t^{(n)}}{\sigma_K} \right) \frac{d}{dy} K^{(n+1)} \right) \right] \tag{B12}$$

$$\varepsilon^{(n+1)} = \varepsilon^{(n)} + \Delta t \left[\frac{C_{\varepsilon_1}^{*(n)} \mathcal{P}^{(n)} - C_{\varepsilon_2} \varepsilon^{(n+1)}}{\tau_c^{(n)}} + \frac{d}{dy} \left(\left(1 + \frac{\nu_t^{(n)}}{\sigma_\varepsilon} \right) \frac{d}{dy} \varepsilon^{(n+1)} \right) \right] \tag{B13}$$

with

$$C_{\varepsilon 1}^{*(n)} = C_{\varepsilon 1} \left(1 + a_1 \frac{\mathcal{P}^{(n)}}{\varepsilon^{(n)}} \right), \quad \nu_t^{(n)} = C_\mu \tau_{22}^{(n)} \tau_c^{(n)} . \tag{B14}$$

The boundary conditions were implicitly written for ε as

$$\varepsilon^{(n+1)} = 2 \frac{K^{(n+1)}}{y_1^2} . \tag{B15}$$

References

Durbin, P. A. 1991. Near-wall turbulence closure without 'damping functions'. *Theoret. Comput. Fluid Dyn.* **3**, 1–13.

Durbin, P. A. 1993a. A Reynolds stress model for near-wall turbulence. *J. Fluid Mech.* **249**, 465–498.

Durbin, P. A. 1993b. Application of a near-wall turbulence model to boundary layers and heat transfer. *Int. J. Heat and Fluid Flow* **14**, 316–323.

Durbin, P. A. 1995. Separated flow computations with the $K-\varepsilon-\overline{v}^2$ model. *AIAA J.* **33**, 659–664.

Gatski, T. B. and Jongen, T. 2000. Nonlinear eddy viscosity and algebraic stress models for solving complex turbulent flows. *Progress in Aerospace Sciences*, **36**, 655–682.

Hanjalić, K. 1994. Advanced turbulence closure models: a view of current status and future prospects. *Int. J. Heat and Fluid Flow* **15**, 178–203.

Manceau, R. 2000. Reproducing the blocking effect of the wall in one-point turbulence models. *Proceedings of the European Congress Comput. Meth. Appl. Sciences and Engineering*, Barcelona, Spain.

Manceau, R., Carlson, J. R. and Gatski, T. B. 2001. A Rescaled Elliptic Relaxation Approach: Neutralizing the Effect on the Log-Layer. Submitted to *Phys. Fluids.*

Manceau, R. and Hanjalić, K. 2000. A new form of the elliptic relaxation equation to account for wall effects in RANS modeling. *Phys. Fluids*, **12**, 2345–2351.

Moser, R. D., Kim, J. and Mansour, N. N. 1999. DNS of Turbulent Channel Flow up to Re_τ=590. *Phys. Fluids*, **11**, 943–945.

Pettersson Reif, B. A., Durbin, P. A. and Ooi, A. 1999. Modeling rotational effects in eddy-viscosity closures. *Int. J. Heat and Fluid Flow* **20**, 563–573.

So, R. M. C., Lai, Y. G., Zhang, H. S., and Hwang, B. C. 1991. Second-order near-wall turbulence closures: a review. *AIAA J.* **29**, 1819–1835.

Speziale, C. G., Sarkar, S. and Gatski, T. B. 1991. Modeling the pressure-strain correlation of turbulence: an invariant dynamical systems approach. *J. Fluid Mech.* **227**, 245–272.

Wizman, V., Laurence, D., Kanniche, M., Durbin, P. and Demuren, A. 1996. Modeling near-wall effects in second-moment closures by elliptic relaxation. *Int. J. Heat and Fluid Flow* **17**, 255–266.

REPORT DOCUMENTATION PAGE

Form Approved
OMB No. 0704–0188

1. AGENCY USE ONLY *(Leave blank)*	2. REPORT DATE	3. REPORT TYPE AND DATES COVERED
	July 2002	Technical Memorandum

4. TITLE AND SUBTITLE
Elliptic Relaxation of a Tensor Representation for the Redistribution Terms in a Reynolds Stress Turbulence Model

5. FUNDING NUMBERS
706-31-11-06

6. AUTHOR(S)
J. R. Carlson and T. B. Gatski

7. PERFORMING ORGANIZATION NAME(S) AND ADDRESS(ES)
NASA Langley Research Center
Hampton, VA 23681–2199

8. PERFORMING ORGANIZATION REPORT NUMBER
L–18197

9. SPONSORING/MONITORING AGENCY NAME(S) AND ADDRESS(ES)
National Aeronautics and Space Administration
Washington, DC 20546–0001

10. SPONSORING/MONITORING AGENCY REPORT NUMBER
NASA/TM–2002–211750

11. SUPPLEMENTARY NOTES

12a. DISTRIBUTION/AVAILABILITY STATEMENT
Unclassified-Unlimited
Subject Category 34 Distribution: Nonstandard
Availability: NASA CASI (301) 621–0390

12b. DISTRIBUTION CODE

13. ABSTRACT ***(Maximum 200 words)***
A formulation to include the effects of wall proximity in a second-moment closure model that utilizes a tensor representation for the redistribution terms in the Reynolds stress equations is presented. The wall-proximity effects are modeled through an elliptic relaxation process of the tensor expansion coefficients that properly accounts for both correlation length and time scales as the wall is approached. Direct numerical simulation data and Reynolds stress solutions using a full differential approach are compared for the case of fully developed channel flow.

14. SUBJECT TERMS
Turbulence Modeling, Elliptic Relaxation, Tensor Representations

15. NUMBER OF PAGES
23

16. PRICE CODE

17. SECURITY CLASSIFICATION OF REPORT	18. SECURITY CLASSIFICATION OF THIS PAGE	19. SECURITY CLASSIFICATION OF ABSTRACT	20. LIMITATION OF ABSTRACT
Unclassified	Unclassified	Unclassified	